CHAPTER II

LITERATURE REVIEW

2.1 Basic Principles of Photocatalysis

Photocatalysis can be defined as the speeding up of a photoreaction by using the catalyst (Mills and Hunte, 1997). This technique is based on the interaction between a catalyst and the UV radiation. There are many semiconductors having potential for photocalytic reaction as indicated by the band gap energy (Table 2-1).

Table 2-1 Band gap energy of various photocatalysts (Bhatkhande et.al, 2001)

Photocatalyst	Band gap energy (eV)
TiO_2 (anatase)	3.2
TiO_2 (rutile)	3.0
ZnO	3.2
WO_3	2.7
SnO_2	3.5
Fe_2O_3	2.2
α-Fe_2O_3	3.1

Photocatalysis over a metal oxide such as TiO_2 is initiated by the absorption of a photon with energy equal to or greater than the band gap (3.2 eV for TiO_2), producing electron-hole (e^-/h^+) pairs. The mechanism of photocatalytic degradation is shown in Figure 2-1. A photon photon with energy of hv exceeds the energy of the band gap, an electron (e^-) is promoted from the valence band to the conduction band leaving a hole (h^+) behind. Electron-hole pairs are diffused and trapped at the surface of the catalytic particle and take part in the chemical reaction with the adsorbed donor (D) or acceptor (A) molecules. The holes can oxidize donor molecules (Equation 2-1) whereas the conduction band electrons can reduce appropriate electron acceptor molecules (Equation 2-2).

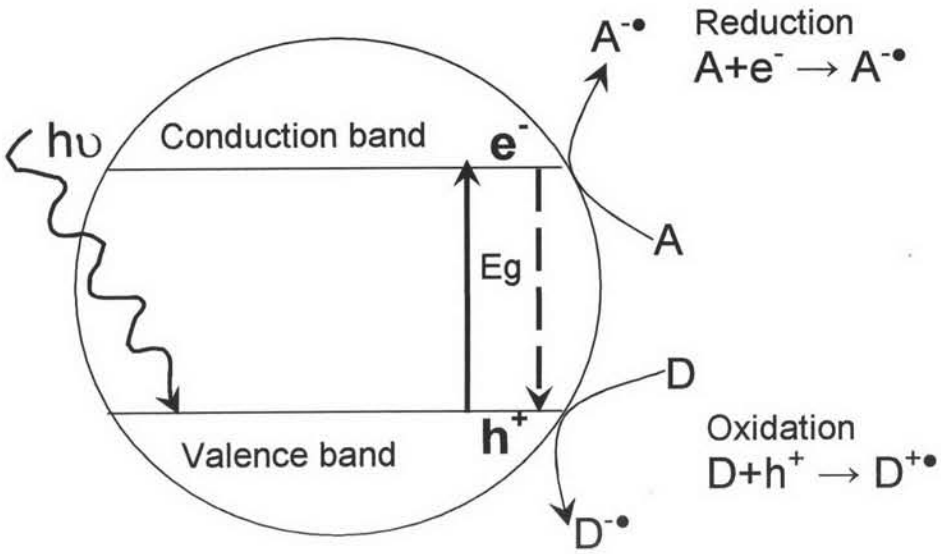

Figure 2-1 Schematic of photocalytic reaction of TiO_2 when it was irradiated.

$$D + h^+ \rightarrow D\bullet+ \quad \text{.....(2-1)}$$

$$A + e^- \rightarrow A\bullet- \quad \text{.....(2-2)}$$

A characteristic feature of metal oxides catalyst is the strong oxidation power of their holes (h^+). They can react in a one-electron oxidation step with water (Equation 2-3) to produce the highly reactive hydroxyl radical (•OH). Both the holes and the hydroxyl radicals are very powerful oxidants, which can be used to oxidize most organic contaminants.

$$H_2O + h^+ \rightarrow \bullet OH + H^+ \quad \text{.....(2-3)}$$

In general, air oxygen acts as electron acceptor (Equation 2-4) by forming the super-oxide ion ($O_2\bullet-$). Superoxide ions are also highly reactive particles, which are able to oxidize organic materials.

$$O_2 + e^- \rightarrow O_2\bullet- \quad \text{.....(2-4)}$$

However, the photo-induced charge separation in bare TiO_2 particles has a very short lifetime because of charge recombination (Sumita et al., 2002). Therefore, it is better to prevent electron-hole recombination to improve the efficiency of photocatalytic reaction. Retardation the recombination of the electron-hole could be performed by using the composite material with various transition metal ion, thus lead to enhancing the efficiency of the photocatalytic systems (Carp et al., 2004).

2.2 Titanium dioxide as Photocatalyst

Titanium dioxide (TiO_2) is one of the most widely studied photocatalysts for environmental applications due to its nontoxic nature and chemical stability. It has attracted much interest during the past decade due to its ability to photo-oxidize of harmful organic compounds in both polluted air and water in the presence of UV light (Fox and Dulay, 1993; Hoffmann et al., 1995; Linsebigler et al., 1995; Mills and Hunte, 1997; Litter, 1999; Watanabe et al., 1999; Tryk et al., 2000; Bhatkhande, 2001; Carp et al., 2004; Devipriya and Yesodharan, 2005).

Titanium dioxide, also known as titanium (IV) oxide or titania, is the naturally occurring oxide of titanium. It has four forms which are rutile (tetragonal), anatase (tetragonal), brookite (orthorhombic), and titanium dioxide (B) (monoclinic) (Carp et al., 2004). However, rutile and anatase usually employ in the applications of photocatalysis due to their band gap energy corresponded to the energy of UV region (λ<380 nm) to create an electron hole pair (Table 2-2). Regarding the structures of both rutile and anatase, the basic building block consists of a titanium atom surrounded by six oxygen atoms in a more or less distorted octahedral configuration. In addition to the rutile, the neighboring octahedra share one corner along (110) planes. While for anatase, the corner-sharing octahedra form (001) planes (Figure 2-12) (Diebold, 2003).

Table 2-2 Bulk properties Titanium dioxide (Diebold, 2003)

Crystal structure	Band gap (eV) (Carp et al., 2004)	System	Lattice constant (nm)	
			a=b	c
Rutile	3.0	Tetragonal	0.4584	0.2953
Anatase	3.2	Tetragonal	0.3782	0.9502

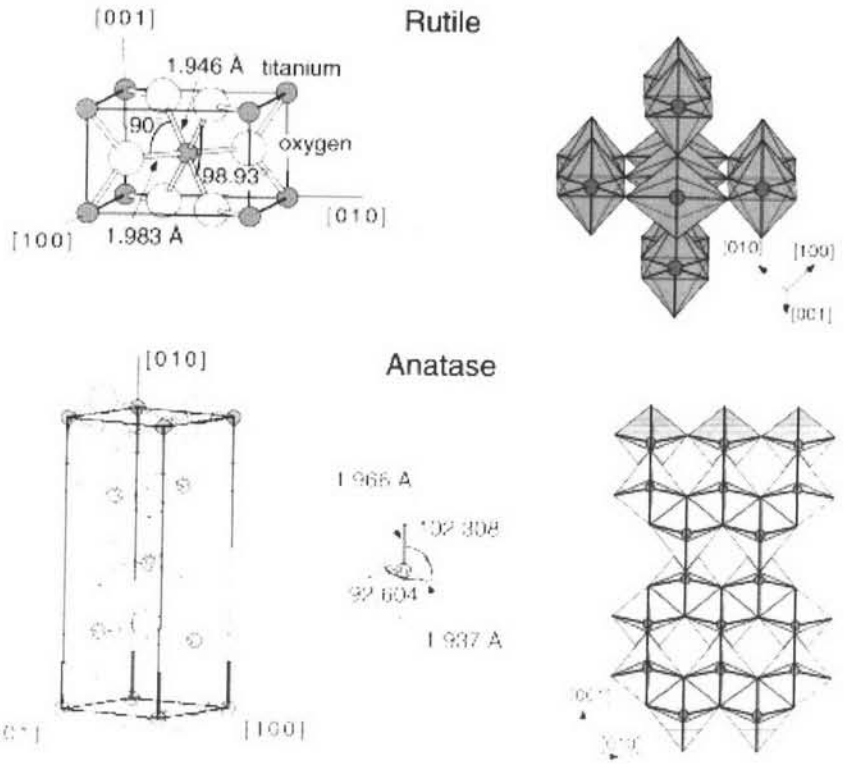

Figure 2-2 Bulk structures of rutile and anatase (Diebold, 2003)

2.3 Sol-Gel Technique

Sol-gel is the popular technique for preparing nanocrystalline of titanium dioxide since this process control the structure of a material on a nanometer scale from the earliest stage of processing. This process also yields extremely pure materials and homogeneity (Hench and West, 1990).

"Sol" is defined as a colloidal suspension of a solid in a liquid medium while a "gel" is defined as a colloidal suspension of a liquid in a solid medium. "Sol" and "gel" are formed in the intermediate stages of the process of forming metal oxides from metal alkoxide precursors. Thus this process is typically termed as "Sol-gel" process. In most cases, the process involves the hydrolysis and polymerization of metal alkoxide precursors and subsequent formation of the gel, resulting in a crystalline network structure after heat treatment (Klein, 1997). The sol-gel process is the formation of gel at the first stage, which consists of growing metal-oxide chains surrounding solvent

molecules. Gelation is succeeded by the formation of additional metal-oxide crosslink, which pull chains together and result in shrinkage of the gel. This contraction brings additional –OH groups together, resulting in further condensation. The next stage of the sol-gel process is aging, which involves the loss of water, solvent and any alcohols produced during hydrolysis and condensation (Brinker and Scherer, 1990).

2.4 Transformation of Anatase-Rutile Phase

In general, the anatase phase of TiO_2 has been recognized to perform the higher activity of photocatalysis (Watanabe, 1999; Sumita et al., 2002). There are some reports mentioned that mixed phases of anatase and ruilte tend to exhibit a higher photoactivity than a single phase of anatase. Chen et al (2006) proposed that there is a nano-structured morphology comprised of rutile crystallites interwoven with anatase crystallites creating a solid–solid interface across, of which photo-excited electrons are transferred from rutile to lower energy anatase lattice trapping sites. Because of its smaller band gap (3.0 eV), rutile acts as an antenna to extend the photo response of the mixed phase catalyst into the visible light region. Its association with anatase in a preferred nanostructured arrangement results in spatial separation of the charge carriers and hindered recombination. Hurum et al (2003;2006) documented that recombination reactions are dominated by surface reactions following charge migration via a random flight mechanism. Figure 2-3 demonstrates illumination promoting an electron into the rutile conduction band. This electron is then located sequentially in trapping sites in (1) the rutile lattice, (2) the anatase lattice, and (3) interfacial and surface sites.

Chen et al (2006) also identified an interfacial, tetahedrally coordinated Ti^{4+} site as an electron trapping site that is specific to mixed phase materials such as Degussa P25 which is a commonly studied formulation of TiO_2, consisting of a mixture of ~80% anatase and ~20% rutile mineral phases. This formulation has been found to be particularly active in oxidizing organic compounds. This site may be created at the solid–solid interface between the nano-particles of mixed phase TiO_2 and responsible

for its high activity. Due to the reason above, the literature on the effects that can cause the antase-to-rutile transformation are reviewed subsequently.

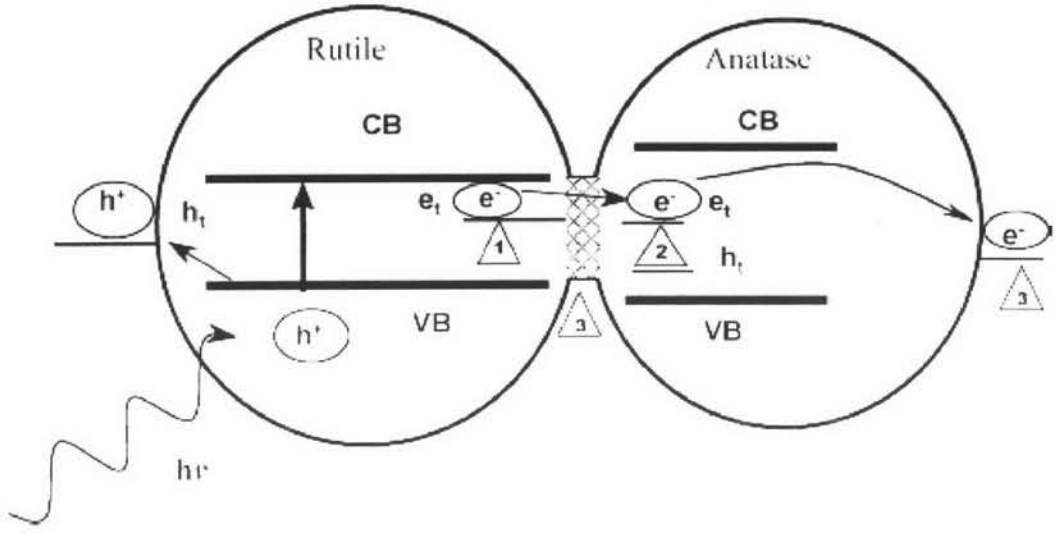

Figure 2-3 Proposed conceptual model of high activity mixed phase catalyst by Hurum et al. (2006).

2.4.1 Effect of Heat Treatment

Anatase can be transformed to Rutile at the upraised temperatures, the transformation being exothermic; reaction that release energy in the form of heat. Navrotsky and Kleppa (1967) investigated the enthalpy of the anatase to rutile transformation the result showed a negative value which means anatase is metastable with respect to rutile under all conditions of temperature and pressure. This according to the JANAF thermochemical data (Chichina and Thicy, cited in Stall, 20005), which is shown in Figure 2-4. The JANAF data shows the free energy of rutile is always less than that of anatase, making rutile is more stable structure at all examined temperatures.

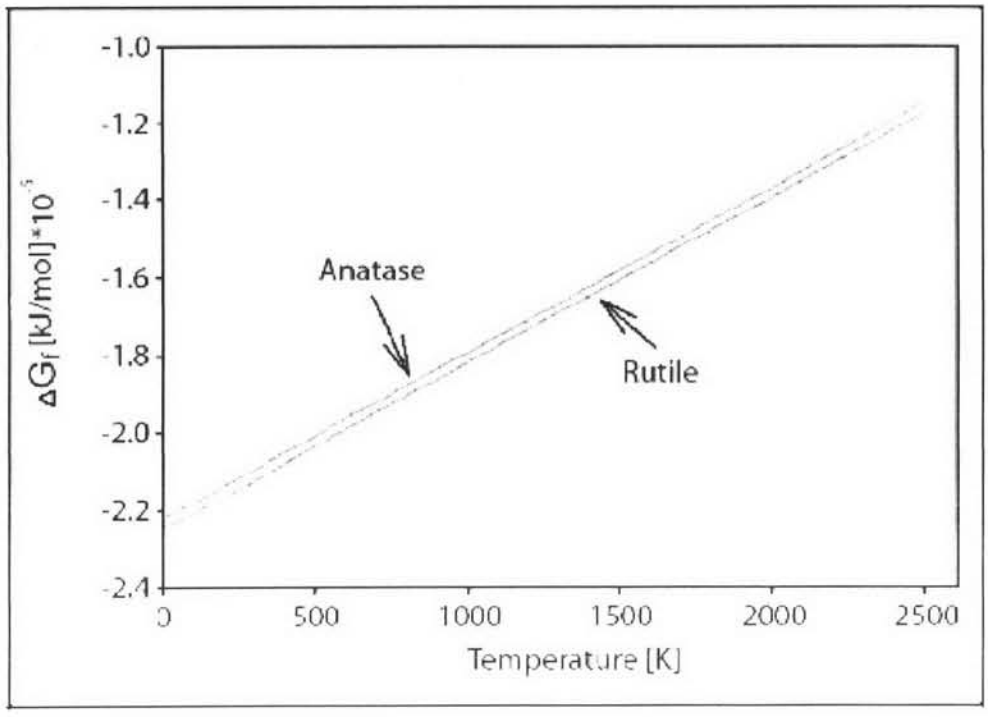

Figure 2-4 Free energy of formation of anatase and rutile phase as a function of temperature (Chichina and Thicy, cited in Stall, 2005).

Li et al. (2002) showed their results that crystallization appears just after drying of precursor and the phase structure of the powder calcined at temperatures below 600 °C is mainly of anatase type. The phase transformation from anatase to rutile occurred at about 600 °C and completed at about 800 °C. A lower phase transformation was found by Su et al. (2004). Their results showed that a calcination temperature of 400 °C, only anatase phase was observed. As calcination temperature was increased to 700 °C, the rutile phase became the major constituent of TiO_2. Jung et al. (2005) reported that increasing the calcination temperature not only effected to anatase-to-rutile transformation but also conveyed to the reduction of structural irregularity, which means that the prepared titania is turned into more ordered crystalline.

2.4.2 Effect of Dopants

Since the study of Shannon and Pask (1965) published, it is clear that dopants (a little added substances) are an important effect of anatse-to-rutile transformation. Richards (2002) concluded that the retardation of anatase-rutile transformation could

be achieved by the following dopants: PO_4^{-3}, SO_4^{-2}, Al^{+3}, $AlPO_4$, SiO_2, Co_3O_4, MoO_3, Ce, Nb, K^+, WO_3, Na_2O, and P_2O_5. Conversely, it is well known that other dopants enhance the formation of rutile at the lower temperature. These dopants include CuO_2, V_2O_5, NiO, CoO, MnO_2 and Fe_2O_3. He also explained that oxygen vacancies are responsible for the overall transformation mechanism. Thus, the oxides and fluorides (e.g. Li^{+1}, Co^{+2} and Mn^{+4}) that assist the transformation can substitute for Ti^{+4} in the anatase lattice, resulting in the creation of oxygen vacancies. On the other hand, the inhibiting effect of other dopants (PO_4^{-3}, SO_4^{-2}, Nb_2O_5) had been explained by the reduction of oxygen vacancy due to the substitution of Nb^{+5} and S^{+6} into the anatase lattice.

2.4.3 Effect of Precursor

The effect of precursor on the resulting crystal structure of titanium dioxide has not been comprehensive. Nevertheless, there are a few reports by Zheng et al. (2001) that PVP affect on the gelation time and lower the onset temperature of anatase-to-rutile transformation. Music et al. (1996) reported that the phase composition of the products of aging of the TiO_2 precursor depends on its colloidal state (polymer, sol, gel or precipitate). Additional stabilization of TiO_2 colloids can be achieved with polymers, e.g. hydroxypropyl cellulose (HPC) and polyethylene glycol (PEG). These polymers also prevent sintering of particles during the heat treatment.

2.5 Composite Titanium dioxide and Tin oxide

One of the methods to improve the activity of the TiO_2 catalyst is to decrease the recombination of photogenerated charge carriers. Coupling TiO_2 with other metal oxides provide a suppressing the recombination of the photogenerated electron hole pairs (Pilkenton and Raftery, 2003). A variety of metal oxides used for coupling TiO_2 are SnO_2, WO_3, Fe_2O_3, ZnO, etc. This study was conducted for the coupling of TiO_2 with SnO_2. Both TiO_2 and SnO_2 have similar spectral responses of large band gap as indicated by 3.2 eV and 3.5 eV, respectively (Table 2-3). As the conduction band (CB) of SnO_2 is lower than that of TiO_2 (Figure 2-5), SnO_2 can act as a sink for the photogenerated electrons. Since the holes move in the opposite direction form the

electrons, photogenerated holes can be trapped within the TiO_2 particle thereby making charge separation more efficient.

Table 2-3 Band position of TiO_2 and SnO_2 (Vinodgopal and Kamat, 1995 and Ni et al, 2007)

Metal Oxide	Band gap Energy (eV)	Conduction Band (CB) (eV)*	Valence band (VB) (eV)*
TiO_2 (anatase)	3.2	-0.5	2.7
SnO_2	3.5	0	3.5

* versus normal hydrogen electrode (NHE)

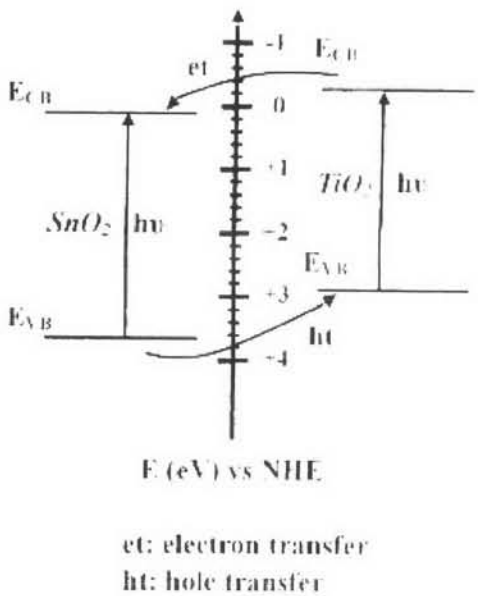

Figure 2-5 Schematic diagram of the charge-transfer in couple metal oxides of TiO_2 and SnO_2 (Shang et al., 2004).

2.6 Phenolic Compounds in Pulp and Paper Wastewater

Pulp and paper industry is one of the large industries that generate a considerable amount of high strength of wastewater. Wastewater characteristics are indicated by high concentration of biochemical oxygen demand (BOD), chemical oxygen demand (COD), suspended solids (SS), toxicity, and color. Moreover, toxic substances in the wastewater are interested as they are potentially harmful to the aquatic ecosystem. Toxic substances are likely produced in the bleaching process where the removal of

residual lignin, a part of the basic structure of wood, has been taken place (Pissololatto et al., 1996). The wastewater from bleaching process thus mostly contains a high amount of various organic compounds. Some organic compounds including phenolic compounds are classified as toxic substances.

In this study, the preliminary determination of pulp and paper wastewater was performed for phenolic compounds (Table 2-5). The real wastewater was collected from the pulp and paper mill. The qualitative analysis by GC/MS presented the structures of organic compounds as shown in Figure 2-6 and Table 2-5. Abundant of the organic compounds were mostly found. The organic compounds also include phenolic compounds; phenol which is the most toxic compound, 2-methoxyphenol (guaiacol) and 2,6-dimethoxyphenol (syringol). In this study phenol, guaiacol and syringol were used as a model of wastewater to evaluate the efficiency of synthesized TiO_2/Sn2. Identification of the intermediate products is an essential prerequisite in the investigation of any reaction mechanisms of organics degradation. Thus, intermediate products after reaction of three phenolic compounds were identified.

Table 2-4 Characteristics of pulp and paper wastewater from preliminary study

Parameters	Characteristic
pH	9.23
COD (mg/l)	1,490
BOD (mg/l)	259
Total Suspended Solid: TSS (mg/l)	980
Total Dissolved Solid: TDS (mg/l)	3,562
Color (Pt Co unit)	2,833
Turbidity (NTU)	330
Total Organic Carbon: TOC (mg/l)	460

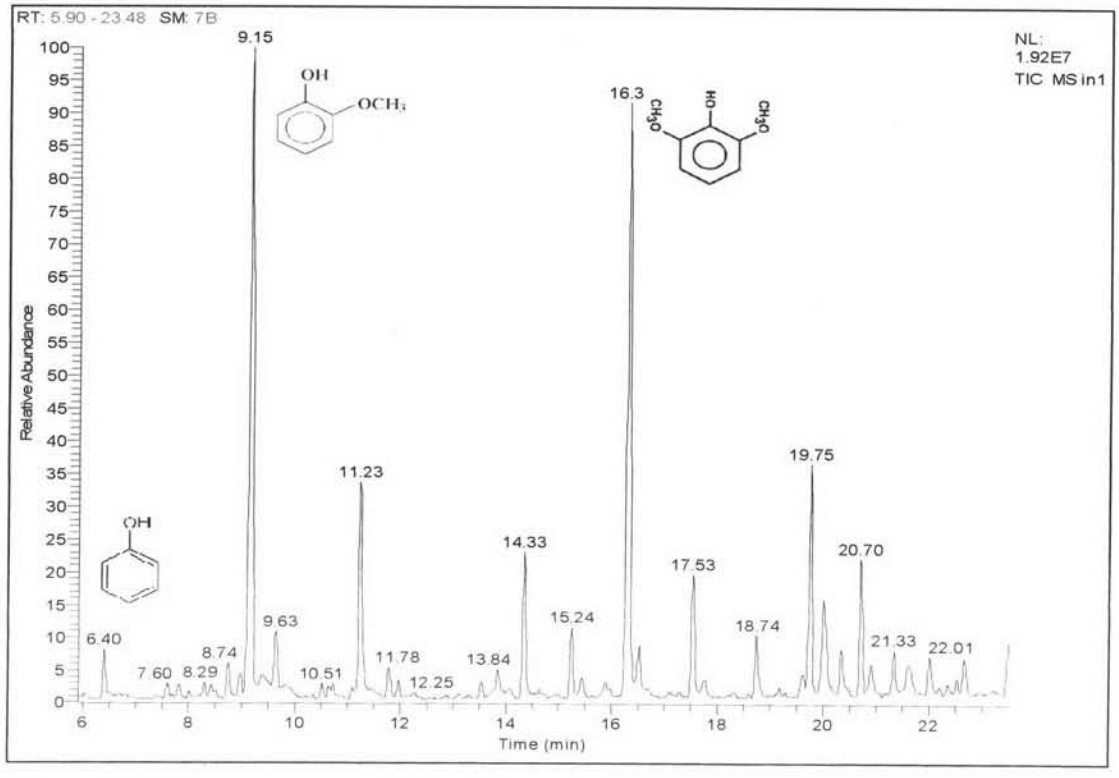

Figure 2-6 Chromatogram of phenolic compounds presented in pulp and paper wastewater from preliminary study.

Table 2-5 Properties of phenolic compounds: phenol, giuaiacol, and syringol presented in pulp and paper wastewater from preliminary study.

Properties	Phenol	Guaiacol	Syringol
Retention time (min)	6.40	9.15	16.30
CAS No.	108-95-2	90-05-1	90-10-1
Molecular formula	C_6H_6O	$C_7H_8O_2$	$C_8H_{10}O_3$
Molecular weight	94	124	154
Hazard code*	Toxic (T)	Harmful (XN)	Harmful (XN)
Main fragments *m/z* (relative abundant)	94(100), 66(31), 65(20), 39(12), 95(7), 55(6), 63(5), 51(4), 50(4), 40(4)	109(100), 124(68), 81(67), 53(22), 52(10), 51(9), 39(7), 110(7), 50(6), 63(6)	154(100), 139(63), 93(53), 96(53), 39(46), 111(44), 15(40), 65(36), 51(29), (53(29)

* European Union Commission Directive 2001/59/EC

2.7 Intermediates products generation

Ohta et al. (1980) investigated catalytic oxidation of phenol in aqueous solution over supported copper oxide (10% CuO on γ–alumina). The color samples in their work turned from transparent to light yellowish brown and finally to heavy blackish brown as conversion of phenol increased. Even if phenol was degraded completely, samples did not become clear and were still blackish brown. The products of phenol oxidation in the solution were identified by using a liquid chromatograph. The intermediates of phenol oxidation were identified as hydroquinone, pyrocatechol, maleic acid, and oxalic acid by a liquid chromatographic technique (Figure2-7). Hydroquinone and pyrocatechol were reported that these intermediates finally disappear after phenol vanished.

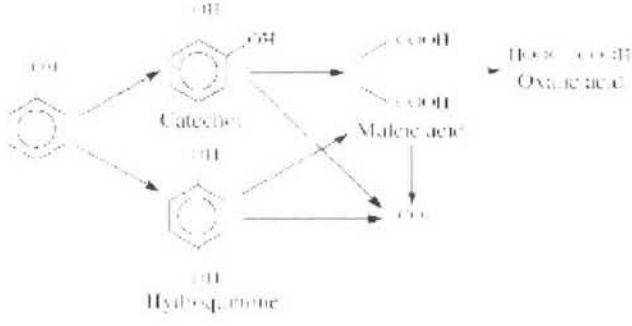

Figure 2-7 Main routes of phenol oxidation purposed by Ohta et al. (1980).

Ding et al. (1995) speculated reaction pathways for the oxidation of phenol in supercritical water (temperature ≈ 450 °C, 500% excess oxygen) that the oxidation of phenol occurs through a sequence of parallel and series reactions as described in Figure 2-8. Path way 2 leads to the formation of partial oxidation products, which can then react further to give the desired product, CO_2. The addition of the MnO_2/CeO or V_2O_5 catalysts is to promote pathway 1 relative to pathway 3 or to enhance the formation of CO_2 through the enhancement of pathways 2 and 4.

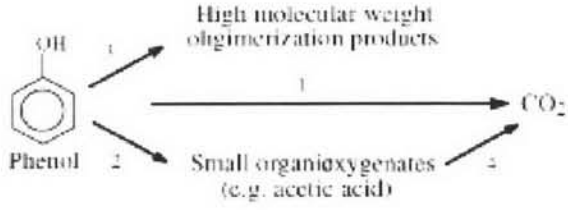

Figure 2-8 Postulated reaction pathways for the oxidation of phenol in supercritical water purposed by Ding et al. (1995).

Devlin and Harris (1984) and Duprez et al. (1996) proposed some intermediate from wet oxidation products of phenol, which were identified in the liquid phase. These intermediates were hydroquinone, catechol and maleic acid which oxidized into acrylic acid and into acetic acid (Figure 2-9). At the end of their experiment, only acetic acid remains in the liquid phase.

Figure 2-9 Schematic of phenol oxidation purposed by Devlin and Harris (1984) and Duprez et al. (1996).

Alejandre et al. (1998) investigated the oxidation of phenol solution by copper oxide catalysts supported on γ-alumina. An aqueous solution of 5 g/l in phenol was oxidized using air as oxidant and a continuous reactor under trickle in periods of eight days. The reaction products were CO_2, diphenols, quinones and organic acids as shown in Figure 2-10. They also reported that polymers can be formed during the phenol oxidation reaction. This homogeneous polymerization reaction markedly reduces the extent of total phenol oxidation and deactivates the catalyst.

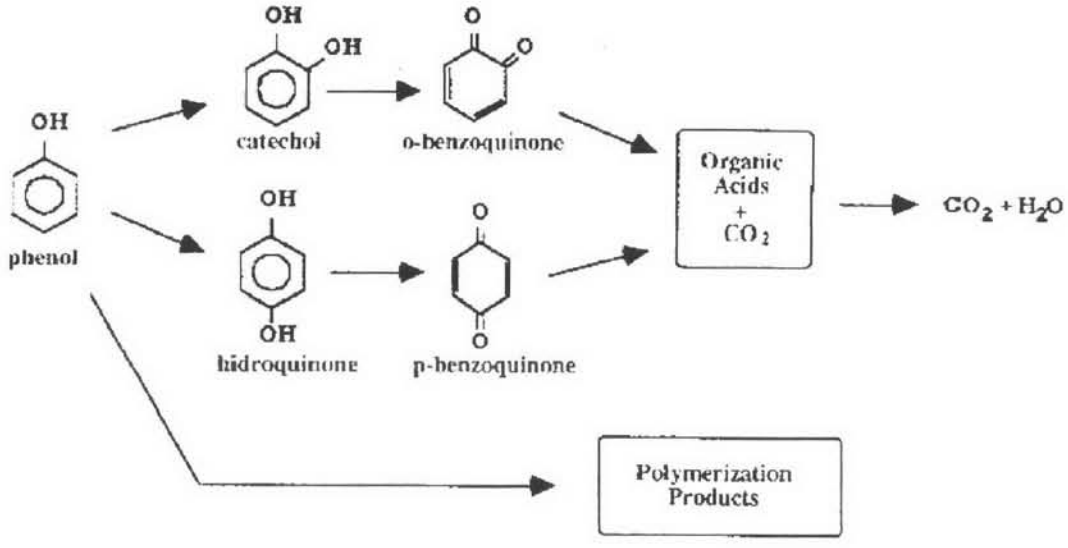

Figure 2-10 Simplified reaction pathway of the phenol oxidation reaction proposed by Alejandre et al. (1998).

Santos et al. (2002) proposed the reaction pathway of phenol oxidation over a copper catalyst (Figure 2-11). The main intermediates detected in the phenol oxidation were ring compounds (hydroquinone, catechol, benzoquinone), which break to yield CO_2 and short chain acids, mainly maleic, formic, acetic and oxalic acids, and also traces of malonic, succinic and fumaric acids. Oxalic acid was also found to form a complex with the copper which oxidizes to CO_2. The only non-oxidizable intermediate under the conditions sets was acetic acid.

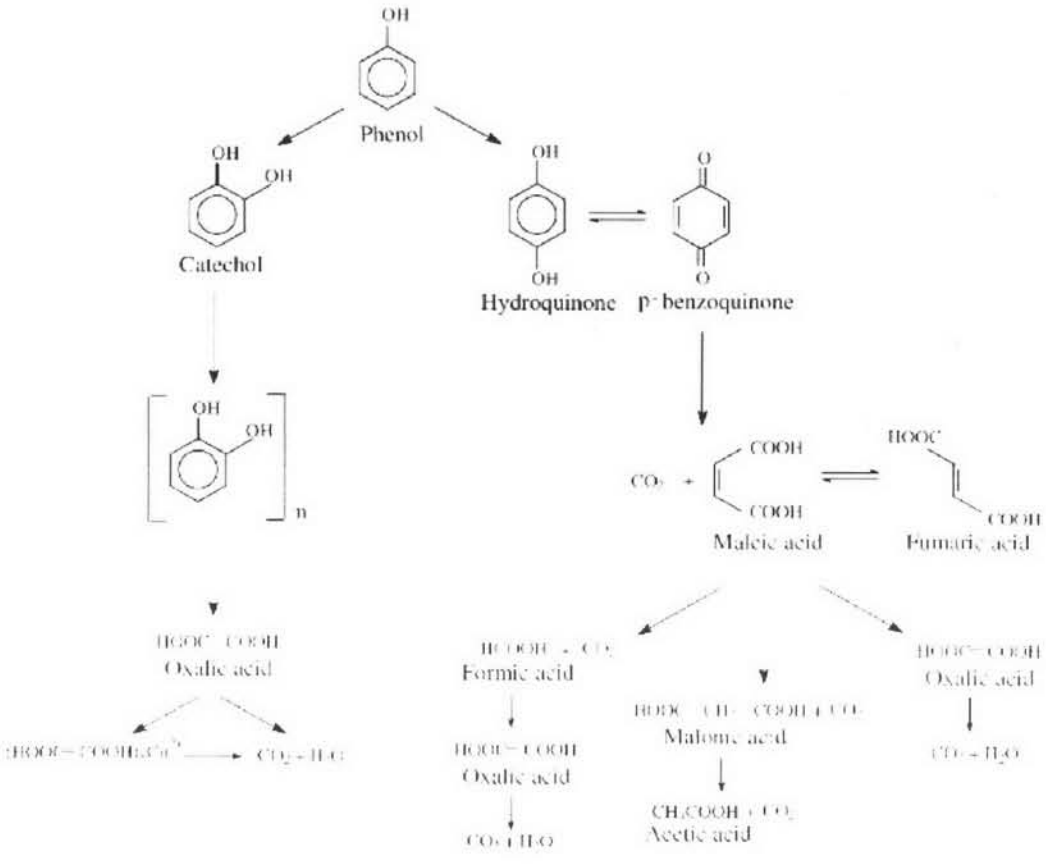

Figure 2-11 Reaction pathway for the phenol oxidation in aqueous phase purposed by Santos et al. (2002).

Nagaveni et al. (2004) investigated the photocatalytic degradation of phenol which was carried out with combustion-synthesized nano-TiO_2 (Figure 2-12). Under identical conditions of UV exposure, the initial degradation rate of phenol with combustion synthesized TiO_2 was double times higher than the initial degradation rate of phenol with commercial Degussa P-25 TiO_2. The intermediates such as catechol (CC) and hydroquinone (HQ) were not detected during the degradation of phenol with combustion-synthesized TiO_2 while both the intermediates were detected when phenol was degraded over Degussa P-25. This indicates that the rates of secondary photolysis of CC and HQ occur extremely faster than the rates at which they are formed from phenol. It further implies that the primary hydroxylation step is rate limiting for the combustion-synthesized TiO_2 aided photodegradation of phenol.

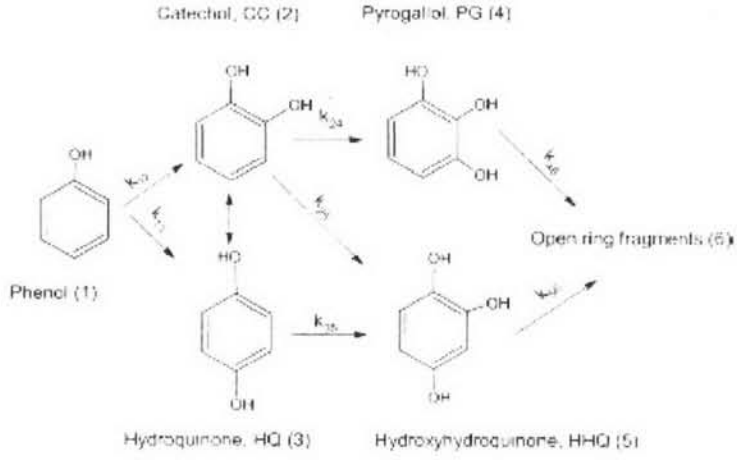

Figure 2-12 Schematic of phenol degradation proposed by Nagaveni et al. (2004).